*IOSR Journal of Electrical and Electronics Engineering (IOSR-JEEE)*
*e-ISSN: 2278-1676,p-ISSN: 2320-3331, Volume 6, Issue 2 (May. - Jun. 2013), PP 38-49*
*www.iosrjournals.org*

# Improved Fuzzy Control Strategy for Power Quality in Distributed Generation's Single Phase Inverters

K. Hanumanth Rao[1], P. Rajasekhar[2], M. Hari Babu[3]
[1, 2, 3](EEE, Vardhaman College of Engineering (Autonomous), JNTU, Hyderabad, India)

***Abstract :*** *Distributed power generation has got its importance with the day to day increase of power generation from renewable energy sources and from domestic customers with small generation units connected to the grid. Distributed power generation systems mostly use Power electronic converters for the interface with power grid. Here in this paper a single-phase inverter for DG systems requiring power quality features, such as harmonic and reactive power compensation for grid-connected operation are discussed. The idea is to integrate the DG unit functions with shunt active power filter capabilities. With this approach, the inverter controls the active power flow from the renewable energy source to the grid and also performs the nonlinear load current harmonic compensation by keeping the grid current almost sinusoidal. The control scheme employs a current reference generator based on sinusoidal signal integrator and instantaneous reactive power (IRP) theory together with a dedicated repetitive current controller. Simulation results obtained with PI and fuzzy controllers demonstrate the feasibility of the proposed solution.*

***Keywords -*** *Distributed power generation, power conditioning, power quality and instantaneous reactive power.*

## I. INTRODUCTION

Recently, due to the high price of oil and the concern for the environment, renewable energy is in the limelight. This scenario has stimulated the development of alternative power sources such as photovoltaic panels, wind turbines and fuel cells [1]–[3]. The distributed generation (DG) concept emerged as a way to integrate different power plants, increasing the DG owner's reliability, reducing emissions, and providing additional power quality benefits [4]. The cost of the distribution power generation system using the renewable energies is on a falling trend and is expected to fall further as demand and production increase.

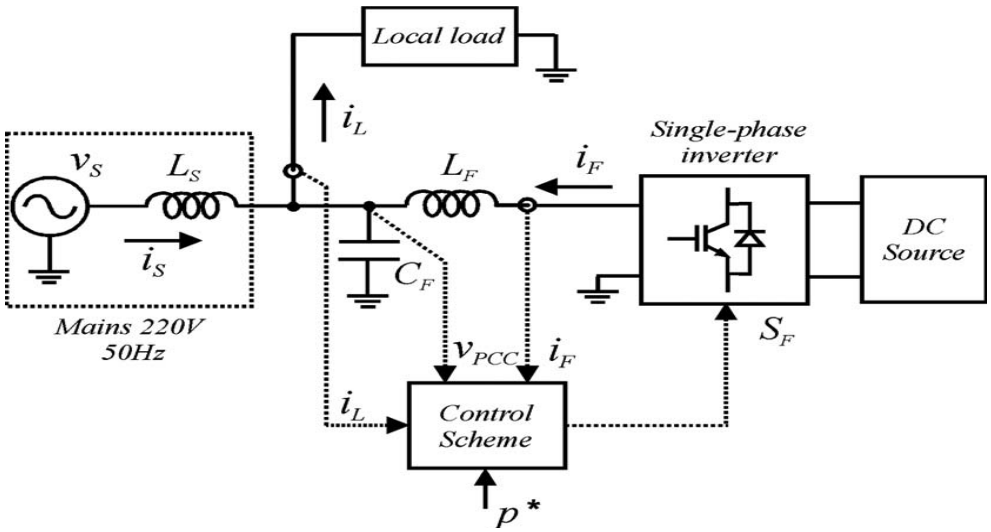


Fig.1 General Scheme of a DG unit connected to the grid.

The energy sources used in DG systems usually have different output characteristics, and for this reason, power electronic converters are employed to connect these energy sources to the grid, as shown in Fig. 1. The power electronic front-end converter is an inverter whose dc link is fed by an ac/dc converter or by a dc/dc converter, according with the DG source type. The commercial front-end inverters are designed to operate either as grid-connected or in island mode. In grid-connected mode, the voltage at the point of common coupling (PCC) is imposed by the grid; thus, the inverter must be current-controlled. When operated in island mode, the inverters are voltage-controlled, generating the output voltage at a specified amplitude and frequency [5], [6].

Coming to the grid-connected mode, almost all the commercial single-phase inverters for DG systems inject only active power to the grid, i.e., the reference current is computed from the reference active power $p^*$ that must be generated [7].

It is possible and can be convenient to integrate power quality functions by compensating the reactive power and the current harmonics drawn by specific local nonlinear loads (see Fig. 1). The single-phase inverter can acquire active filtering features just adding to its control software some dedicated blocks that are specific to shunt active power filter (APF).

This paper proposes and validates an enhanced power quality control strategy for single-phase inverters used in DG systems. The idea is to integrate the DG unit functions with shunt APF capabilities. With the proposed approach, the inverter controls the active power flow from the energy source to the grid and also performs the compensation of reactive power and the nonlinear load current harmonics, keeping the grid current almost sinusoidal.

The integration of APF capability in single-phase inverters needs a particular attention since the control techniques (for example, to find the reference current) were developed for three phase APFs, and consequently, must be adapted for single-phase systems.

The paper is organized as follows. The inverter control scheme is discussed in detail in Section II, with a particular focus on the reference current generator and the current control implementation. Section III is related to the Simulation results and contains a description of the testing setup followed by a complete experimental validation of the proposed control solutions. The simulation results are presented for the grid connected inverter that generates active power and compensates the reactive power and current harmonics of local loads, thus achieving complete power quality features.

## II. INVERTER CONTROL SCHEME

The block diagram of the single-phase inverter control scheme with enhanced power quality features is shown in Fig. 2. The inverter reference current $i_F^*$ is generated by the reference current generator block and the current control is based on a repetitive controller.

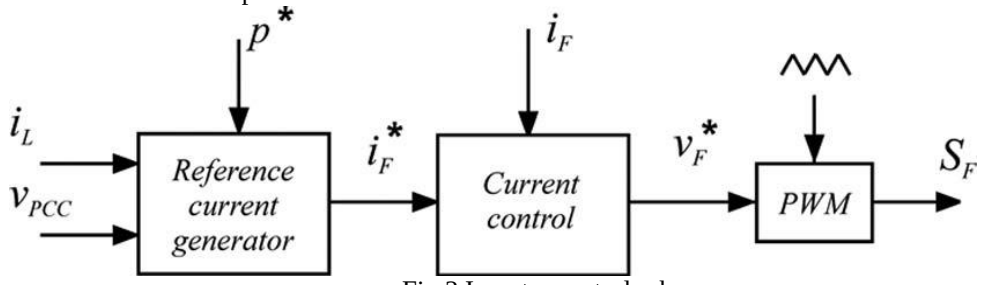


Fig.2 Inverter control scheme.

### 2.1. Reference Current Generator

The reference current generation scheme is shown in Fig. 3 and can be divided into two parts: the computation of the harmonic current reference $i_{h\alpha}$ and the generation of the fundamental reference current $i_{1\alpha}$ corresponding to the active and the reactive power to be generated.

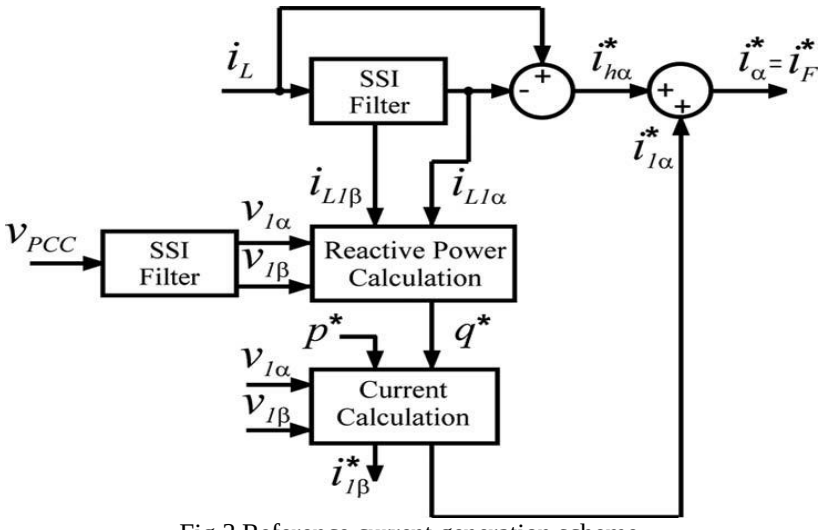


Fig.3 Reference current generation scheme.

### 2.1.1. Generation of the Harmonic Reference Current

The nonlinear load current $i_L$ and the PCC voltage $v_{PCC}$ are used to calculate the reference current for current harmonics compensation. A filter based on SSIs (hereinafter called SSI filter) extracts the fundamental frequency component $\omega 0 = 2\times\pi\times 50$ (in radian per second) of the load current in stationary $\alpha\beta$ frame, as shown in Fig. 3 and Fig. 4 [20]. The harmonic reference current $i_{h\alpha}$ is obtained from the subtraction of the load current from the output of the SSI filter ($i_L - i_{L1\alpha}$).

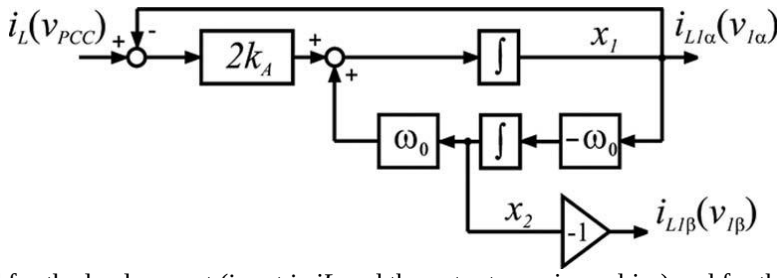


Fig.4 SSI filter applied for the load current (input is *iL* and the outputs are $i_{L\alpha}$ and $i_{L\beta}$) and for the PCC voltage (input is $v_{PCC}$ and outputs are $v_{1\alpha}$ and $v_{1\beta}$ ).

### 2.1.2. Generation of the Fundamental Reference Current

In steady-state operation, the SSI filter shown in Fig. 4 has two sinusoidal states $x_1$ and $x_2$ having the same amplitude and being phase-shifted by 90 electrical degrees [20], [21]. So, it is possible to obtain two outputs from a SSI filter, $i_{L1\alpha}$ and $i_{L1\beta}$ (which is always 90 ◦ shifted respect to $i_{L1\alpha}$ ). This can be seen by analyzing the two transfer functions of the SSI filter.

$$H_1(s) = \frac{I_{L1\alpha}(s)}{I_L(s)} = \frac{2k_A \times s}{s^2 + 2k_A \times s + \omega_0^2} = \frac{V_{1\alpha}(s)}{V_{PCC}(s)} \quad (1)$$

$$H_2(s) = \frac{I_{L1\beta}(s)}{I_L(s)} = \frac{2k_A \times \omega_0}{s^2 + 2k_A \times s + \omega_0^2} = \frac{V_{1\beta}(s)}{V_{PCC}(s)}. \quad (2)$$

In steady-state operation, the relationship between the phases of the transfer functions (1) and (2) in the frequency domain is

$$\angle H_1(j\omega) = \angle H_2(j\omega) + \frac{\pi}{2}. \quad (3)$$

The Bode diagrams of (1) and (2) that are shown in Figs.5 and 6 for different values of $k_a$ confirm (3). It is also possible to see that when $k_A$ becomes smaller, the filter becomes more selective. However, when this happens, the phase delay becomes higher around the fundamental frequency $\omega_0$.

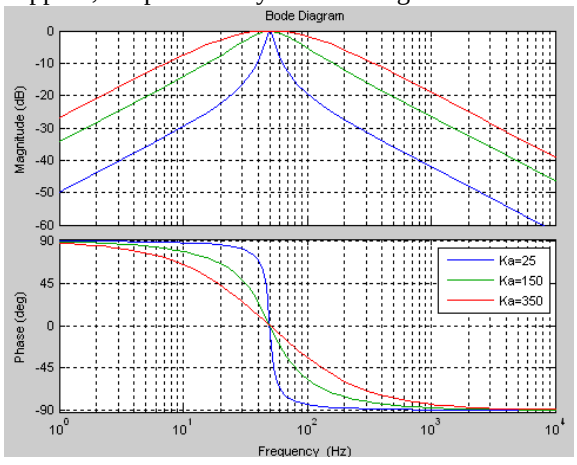


Fig.5 Bode plots of *H*1 (*s*).

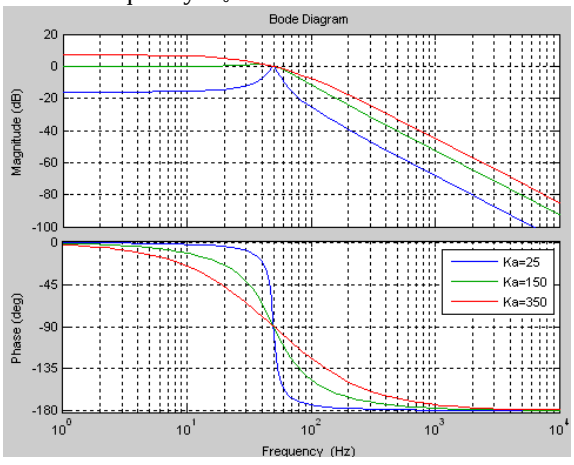


Fig.6 Bode plots of *H*2 (*s*).

This property is useful for obtaining the orthogonal fundamental components needed to perform the reactive power compensation of the local load. The signal $i_{L1\beta}$ is generated by the SSI only to calculate the fundamental reactive power reference $q^*$, using the definition of reactive power from IRP theory as follows:

$$q^* = i_{L1\alpha} v_{1\beta} - i_{L1\beta} v_{1\alpha}. \qquad (4)$$

To obtain $v_{1\alpha}$ and $v_{1\beta}$, another SSI filter is used in the PCC voltage $v_{PCC}$ by generating $v_{1\alpha}$ and a signal ($v_{1\beta}$) with the same amplitude and phase-shifted by 90 electrical degrees from $v_{1\alpha}$, as shown in Fig. 4. The use of an SSI filter in the PCC voltage makes the reference current generator insensitive to grid voltage distortions. The fundamental components of the inverter reference current $i^*_{1\alpha}$ and $i^*_{1\beta}$ are calculated by imposing the reference power $p^*$ equal to the amount of active power to be injected into the grid, as follows:

$$\begin{bmatrix} i^*_{1\alpha} \\ i^*_{1\beta} \end{bmatrix} = \frac{1}{v^2_{1\alpha} + v^1_{1\beta}} \begin{bmatrix} v_{1\alpha} & v_{1\beta} \\ v_{1\beta} & -v_{1\alpha} \end{bmatrix} \times \begin{bmatrix} p^* \\ q^* \end{bmatrix}. \qquad (5)$$

Since the system is single phase, the current $i^*_{1\beta}$ is neglected and $i^*_{1\alpha}$ is added to the harmonic reference current $i^*_{h\alpha}$ to obtain the inverter reference current. The SSI filter used to extract the fundamental component of the nonlinear load current is very flexible, and the gain $k_A$ (see Fig. 4) can be adjusted to improve the selectivity of the reference generator or to improve its transient response.

It is important to emphasize the difference between the solution used in this paper to create the fictitious variable and another existing method [14]. In the proposed technique, the orthogonal fundamental component signals, used for current reference generation and obtained from the SSI filter, are sinusoidal and phase shifted by 90°. In the existing method, the obtained fictitious variable is a signal with a high harmonic content generated by phase shifting all frequencies of the load current by 90°. In this case, some phase delay is introduced in the fictitious variable and implicitly in the inverter current reference [19].

**2.2. Current Control**

For inverters that generate active power and also compensate the reactive power, the reference current is sinusoidal at fundamental frequency, so the use of conventional Fuzzy controllers would probably suffice if their bandwidth is high enough. If the inverter must also compensate the current harmonics, the reference current will become no sinusoidal. In this case, achieving zero –steady-state error is not possible with Fuzzy controllers, unless particular control schemes are employed.

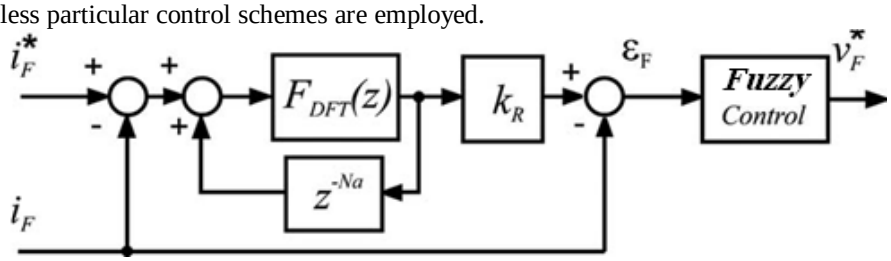


Fig.7 Current control scheme.

Coming to the scheme in Fig. 7, the key issue is the implementation of the repetitive control scheme. The repetitive controller is nothing else than an FIR filter of *N* taps. The filter can be designed by using the discrete Fourier transform (DFT) to achieve unity gain for every single harmonic to be compensated. As described in detail in [22], the filter coefficients can be computed as

$$F_{\mathrm{DFT}}(z) = \frac{2}{N} \sum_{i=0}^{N-1} \left( \sum_{k \in N_h} \cos\left( \frac{2\pi}{N} h(i + N_a) \right) \right) z^{-i} \qquad (6)$$

Where $N$ is the number of the coefficients, $N_h$ is the set of selected harmonic frequencies, and $N_a$ is the number of leading steps necessary to maintain the system stability. The $k_R$ parameter from Fig. 7 influences the repetitive controller speed response [22].

The number of FIR filter taps is directly related to the sampling frequency. To implement (6) with a sampling period $T_s$ of 100 $\mu$s, we will need an FIR filter by using 200 taps. For example, the frequency plots of the FIR filter (6) tuned for the fifth and the seventh harmonics ($N_h$ = 5, 7) and implemented with $N$ = 200 taps are shown in Fig. 8.

The implementation of the original repetitive controller [22] requires a high number of the filter taps that are necessary for the chosen sampling frequency of 10 kHz. To reduce the taps number, a modified repetitive controller is proposed in this paper. The proposed filter coefficients are computed by using

$$F_{\mathrm{DFT}}(z) = \frac{2}{N}\sum_{i=0}^{N-1}\left(\sum_{k\in N_h}\cos\left(\frac{\pi}{N}h(i+N_a)\right)\right)z^{-i}. \quad (7)$$

With respect to (6), the proposed filter (7) allows halving the number of taps for the same sampling frequency. For a sampling frequency of 10 kHz, (7) will lead to $N$ = 100 taps with respect to $N$=200 taps imposed by (6), making the proposed filter more suitable for DSP implementation since the computational time will be significantly reduced.

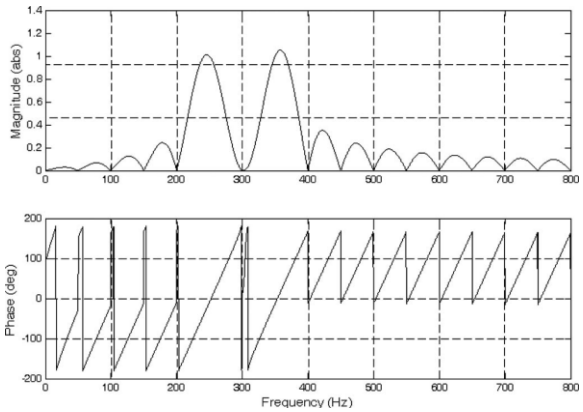


Fig.8 DFT frequency response using $Nh = \{5, 7\}$ and $N$ = 200 taps.

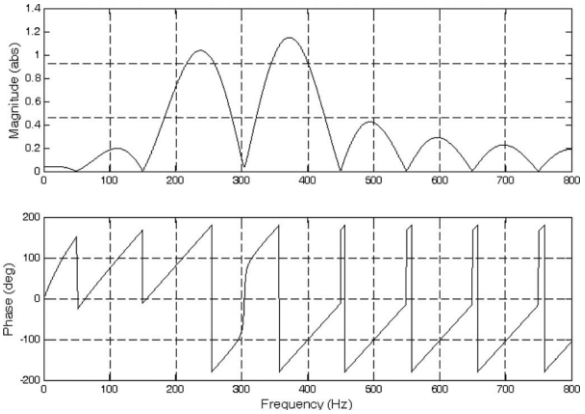


Fig.9 DFT frequency response of the modified FIR filter using $Nh = \{5, 7\}$ for $N$ = 100.

The frequency plots of the proposed FIR filter (7) tuned for the fifth and the seventh harmonics ($N_h$ =5 and 7) and implemented with $N$ = 100 taps are shown in Fig. 9. As can be noted from Fig. 9, the proposed FIR filter exhibits similar filtering properties with the original filter presented in [22], but the implementation is simpler due to the halved number of taps. The number of the leading steps $N_a$ has been set equal to 2 since a mean delay time of 1.5 $T_s$ is introduced by the current control loop, while the $k_R$ parameter has been set equal to 1.

**2.2.1. The Fuzzy current controller**

Table: 1 Fuzzy Membership functions

| **V** | **DEL_V** | **$I_{dr}$** |
|---|---|---|
| NB | NB | NB |
| N | N | N |
| ZE | ZE | ZE |
| P | P | P |
| PB | PB | PB |
| None | None | None |

NB: Negative Big
N : Negative
ZE: Zero
P : Positive
PB: Positive Big

The Fuzzy controller in Fig. 7 has been designed to get a bandwidth of about 700 Hz and a phase margin of 60 electrical degrees. The membership functions of the Fuzzy controller are given in the Table 1.

## III. SIMULATION RESULTS

The general diagram of the setup is shown in Fig. 10, where the positive polarities for grid current $i_S$, load current $i_L$, and inverter current $i_F$ are emphasized, in agreement with Fig. 1. The system parameters are given in Table 2.

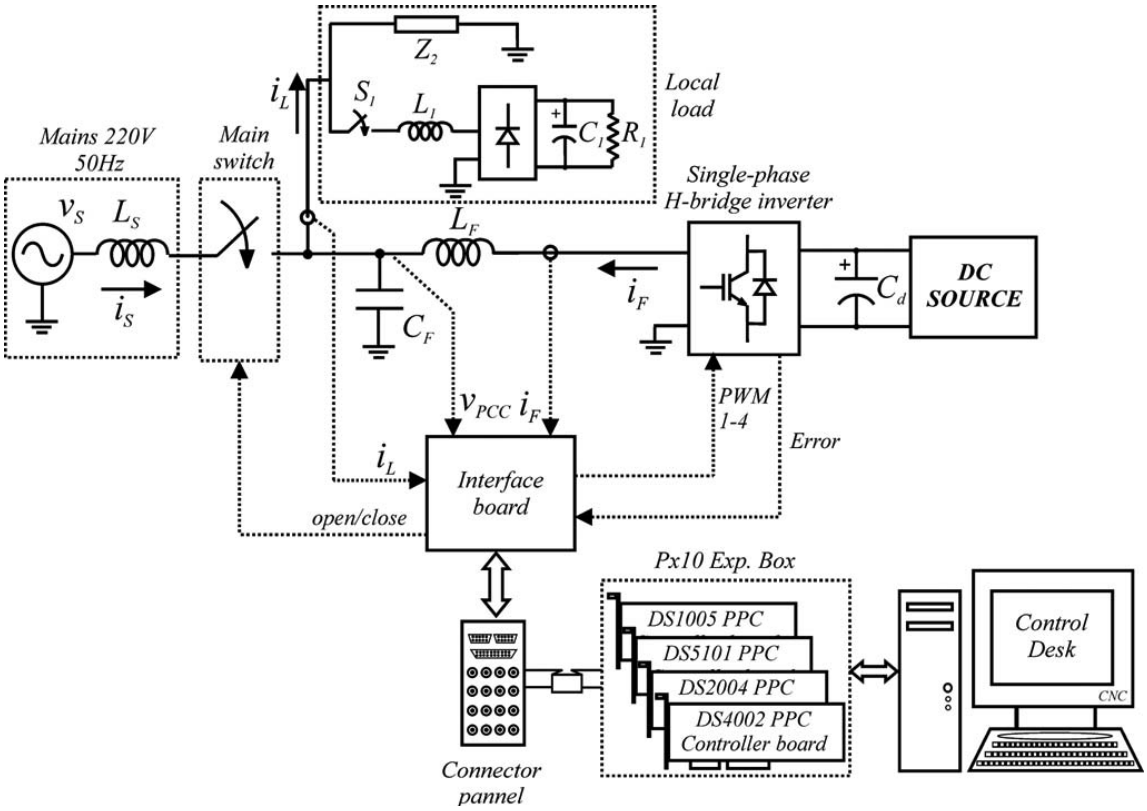


Fig. 10 General diagram of the experimental setup

The hardware platform used to implement the inverter control algorithm is a dSPACE development modular system based on the DS1005 processor board and several boards for each special hardware task (for example, DS 5101 board for pulse width modulation (PWM) generation, DS 2004 board for A/D conversion, and DS 4002 board for digital I/O). All boards are hosted in a dSPACE PX10 expansion box that uses the DS817 board for bidirectional communication with PC through optical fibers.

The repetitive current controller parameters are $k_R = 1$, $N = 100$ (sampling frequency = 10 kHz), $N_h = 2n-1$ with $n = 1,\ldots,13$, and $N_a = 2$. The Fuzzy current controller parameters are $k_p = 3$ and $k_i = 500$.

The quantities measured from the system are the inverter current $i_F$, the PCC voltage $v_{PCC}$, and the local load current $i_L$, as shown in Fig. 10. As the paper focus is on the grid-connected inverter, the dc energy source has been emulated with a three phase diode rectifier fed by a three-phase variance.

Table 2 Simulation Parameters

| Parameter | Symbol | Value |
|---|---|---|
| Mains voltage | $v_S$ | 220 V |
| Interface capacitance | $C_F$ | 7.5 µF |
| Interface inductance | $L_F$ | 700 µH |
| DC-link capacitance | $C_d$ | 2.2 mF |
| DC-link voltage setpoint | $V_{dc}$ | 400 V |
| Switching/Sampling frequency | $f_{sw}, f_s$ | 10 kHz |
| Fundamental frequency | $f_1$ | 50 Hz |
| Linear load resistance | $R_2$ | 25 Ω |
| Linear load inductance | $L_2$ | 30 mH |
| Nonlinear load input inductance | $L_1$ | 900 µH |
| Nonlinear load output capacitance | $C_1$ | 1 mF |
| Nonlinear load output resistance | $R_1$ | 50 Ω |

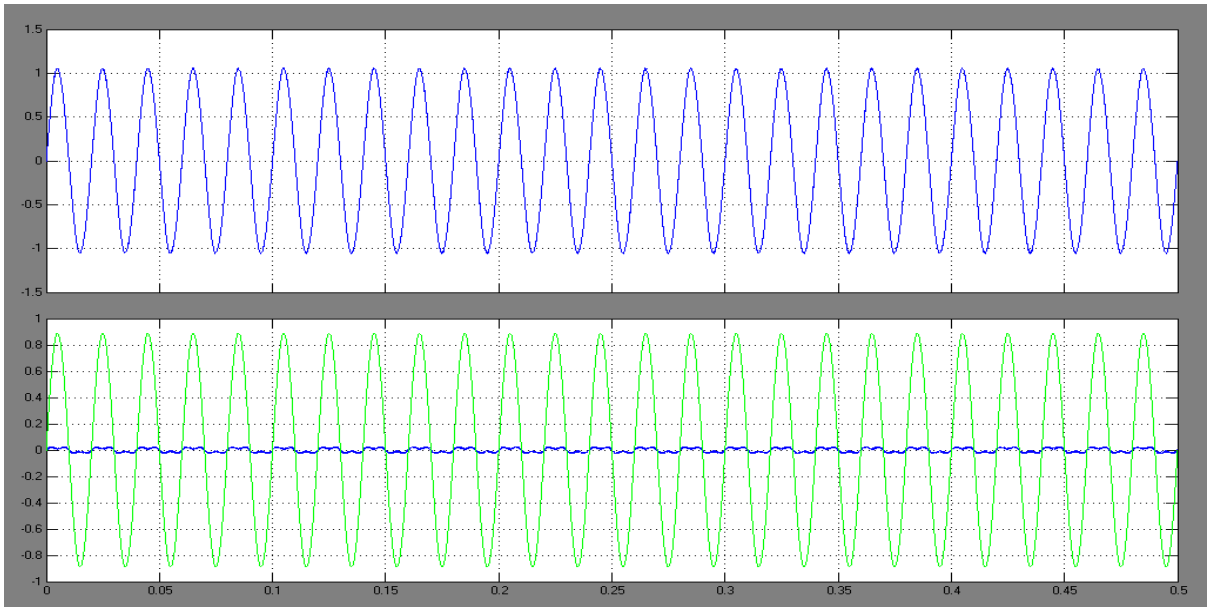

Fig.11 Steady-state operation of the inverter injecting the active power requested by the resistive load (2 kW). (Trace 1) Inverter current $i_F$ (10 A/div). (Trace 2) Grid current $i_S$ (10 A/div). (Trace 3) Grid voltage $v_{PCC}$ (350 V/div).

The single-phase inverter injects active power into the grid and compensates the harmonics generated by a local load, which contains two parts: a 2-kW linear load and a 3-kVA nonlinear capacitive load (a single-phase diode rectifier with capacitive dc load). The linear load ($Z_2$ in Fig. 10) has been considered either as a single resistance ($R_2$) or as a series $RL$ load ($R_2$, $L_2$), whose values are specified in Table 2.

### 3.1. Validation of Active Power Generation

This test has been performed with the inverter having only a 2-kW resistive local load. The steady-state operation for the inverter, injecting 2 kW of active power, is shown in Fig. 11. In this case, it can be seen that the grid current $i_s$ is almost zero because the local load power request is completely supplied by the inverter ($i_S = i_L - i_F$ in Fig. 10).

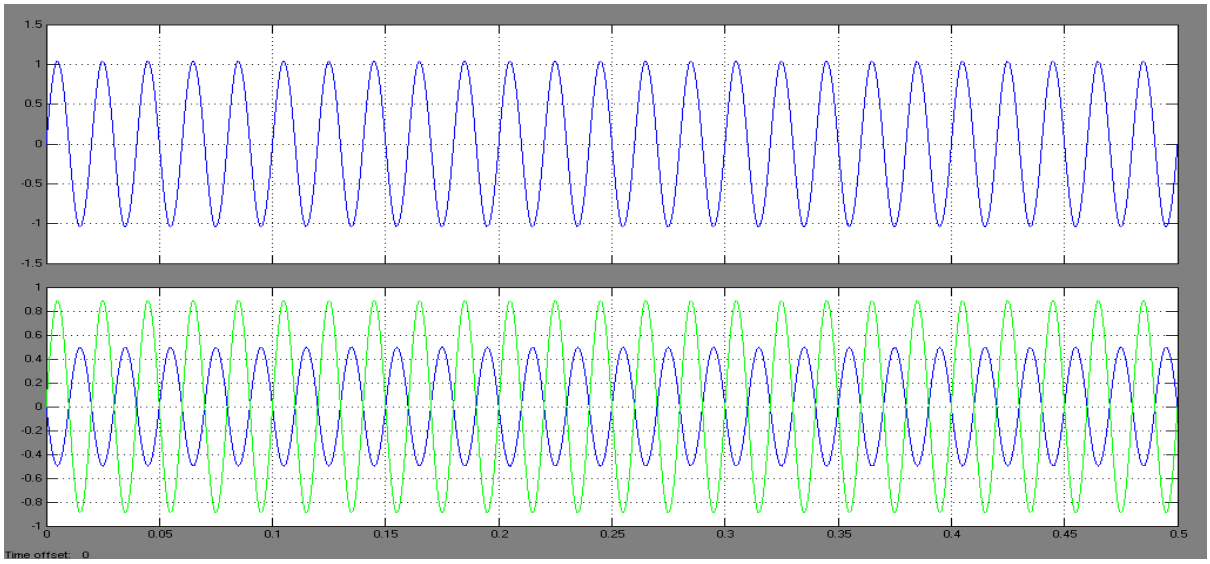

Fig. 12 Steady-state operation for 3 kW active power generation. Only the 2 kW linear load is connected in this case. (Trace 1) Inverter current *iF* (20 A/div). (Trace 2) Grid current *iS* (10 A/div). (Trace 3) Grid voltage *v*PCC (350 V/div).

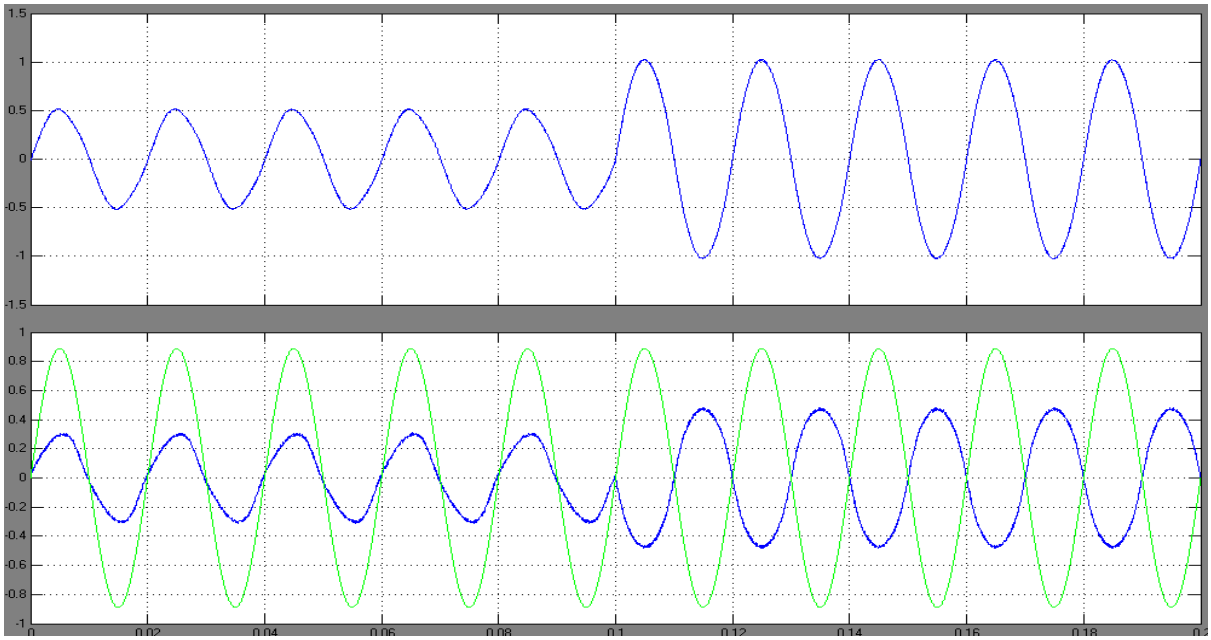

Fig. 13 Inverter transient response during a step-up of the injected active power (1–3 kW). Only the 2 kW linear load is connected. (Trace 1) Inverter current *iF* (20 A/div). (Trace 2) Grid current *iS* (10 A/div). (Trace 3) Grid voltage *v*PCC (350 V/div).

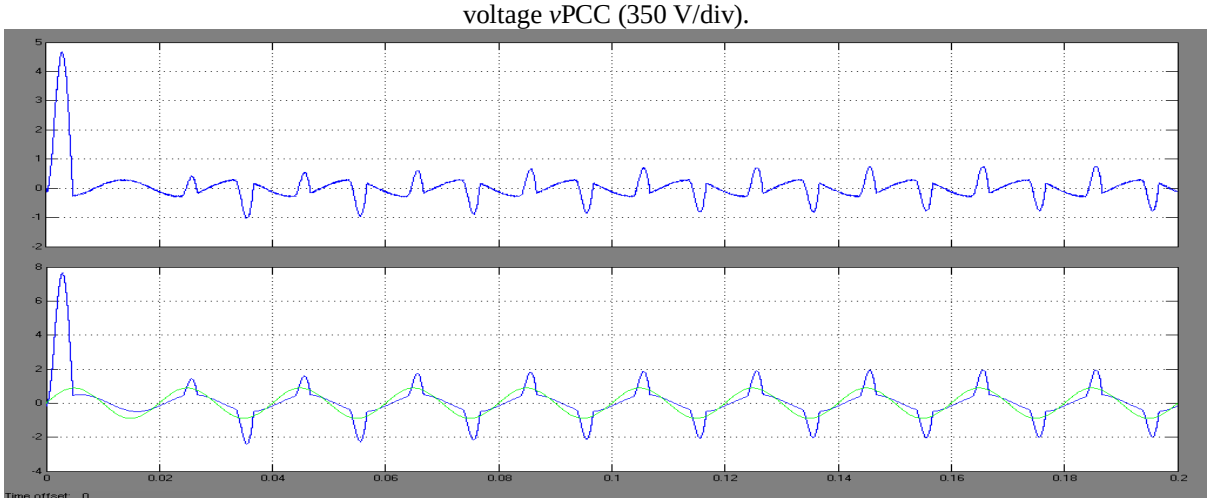

Fig. 14 Steady-state operation of the inverter injecting 1 kW active power and compensating the current harmonics of the local load. (Trace 1) Inverter current *iF* (20 A/div). (Trace 2) Load current *iL* (20 A/div). (Trace 4) Grid voltage *v*PCC (350 V/div).

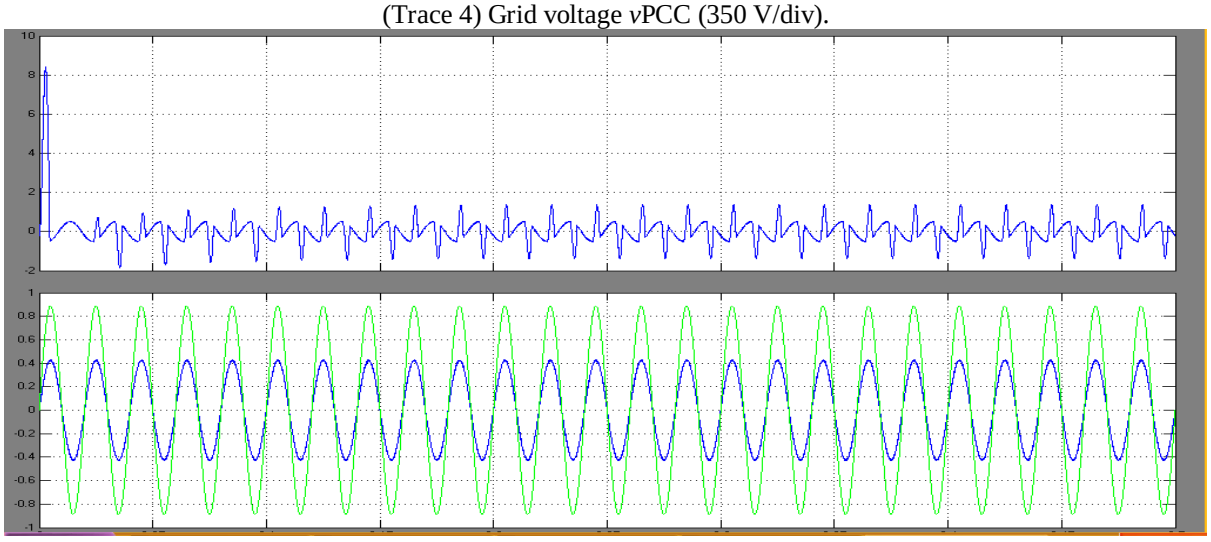

Fig. 15 Steady-state operation of the inverter injecting 1 kW active power and compensating the current harmonics of the local load. (Trace 1) Inverter current *iF* (20 A/div). (Trace 2) Grid current *iS* (40 A/div). (Trace 4) Grid voltage *v*PCC (350 V/div).

### 3.2. Validation of Current Harmonics Compensation

This test has been performed with the inverter having a local load consisted of the resistance $R_2$ and the diode rectifier. The steady-state operation of the inverter, injecting 1 kW of active power and compensating the current harmonics of the local load, is shown in Figs. 14 and 15. The inverter current $i_F$, the PCC voltage $v_{PCC}$, and the local load current $i_L$ are shown in Fig. 14, while Fig. 15 contains the inverter current $i_F$, the PCC voltage $V_{PCC}$, the grid current $i_s$, and the Fourier analysis of the inverter current $i_F$. It can be seen from Figs. 14 and 15 that even if the local load current is highly distorted, the mains current is almost sinusoidal.

Also, it can be noted that the grid current is in phase with the PCC voltage, so in this case, the local load still draws active power from the grid. This happens because the inverter-injected active power of 1 kWis smaller than the active power requested by the local load.

The inverter dynamic performance has been evaluated by turning on the load diode rectifier, as shown in Figs. 16 and 17.

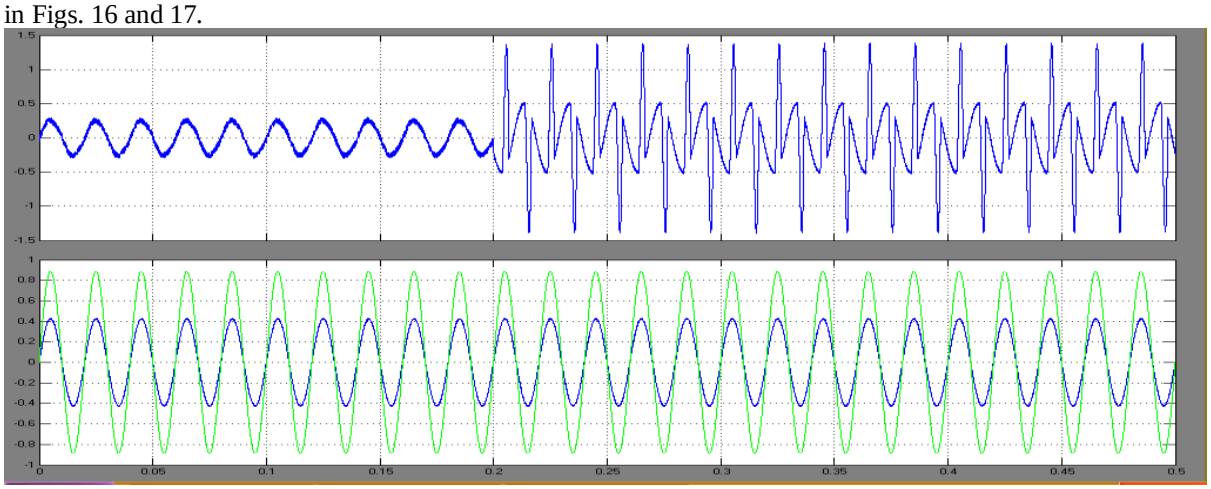

Fig. 16 Inverter transient response during nonlinear load turn-on. (Trace 1) Inverter current *iF* (20 A/div). (Trace 2) Grid current *iS* (40 A/div). (Trace 4) Grid voltage *v*PCC (350 V/div).

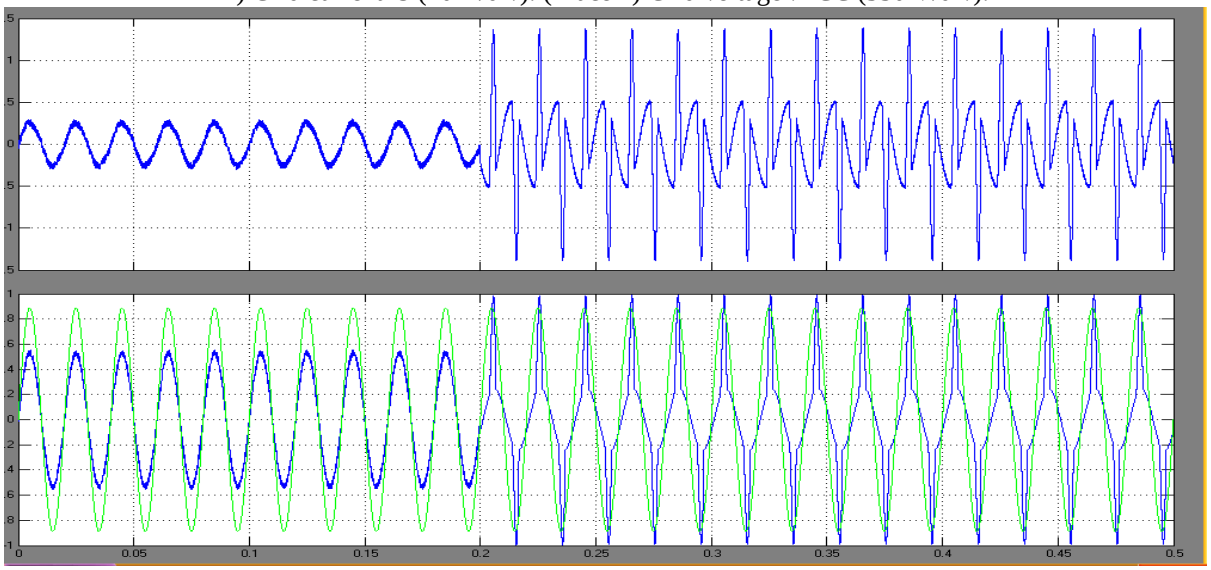

Fig. 17 Inverter transient response for nonlinear load turn-on. (Trace 1) Inverter current *iF* (20 A/div). (Trace 2) Load current $i_L$ (40 A/div). (Trace 4) Grid voltage *v*PCC (350 V/div).

It is resulted from these figures a fast transient response of the inverter with a settling time of about 20 ms.

### 3.3. Validation of Reactive Power Compensation

To clearly emphasize the inverter capability to compensate the local load reactive power, the inverter has been operated only with an *RL* load obtained as the series connection between the resistance $R_2$ and the inductance $L_2$ (Table 2). The load current lags the load voltage by about 20 electrical degrees, as shown in Fig. 19.

The inverter transient operation obtained for zero active power generation when the reactive power is enabled in a step fashion is shown in Fig. 19. It can be noted howthe grid current becomes pure active since the inverter completely compensates the local load reactive power. As expected, the inverter current $i_F$ is pure reactive and leads the PCC voltage by 90 electrical degrees (see Fig. 19).

The steady-state operation of the inverter, injecting 3 kW of active power and compensating the entire load reactive power, is shown in Fig. 20. The grid current is out of phase with respect to the PCC voltage by 180 electrical degrees, which means active power generation since the inverter generates more active power than the active power requested by the load.

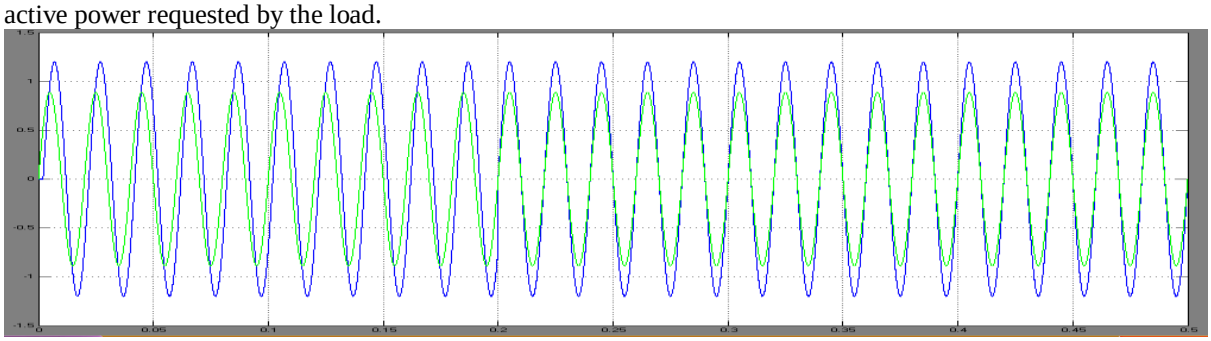

Fig. 18 Steady-state linear resistive–inductive load operation. (Trace 2) Load current *iL* (10 A/div). (Trace 4) Grid voltage $v_{PCC}$ (350 V/div).

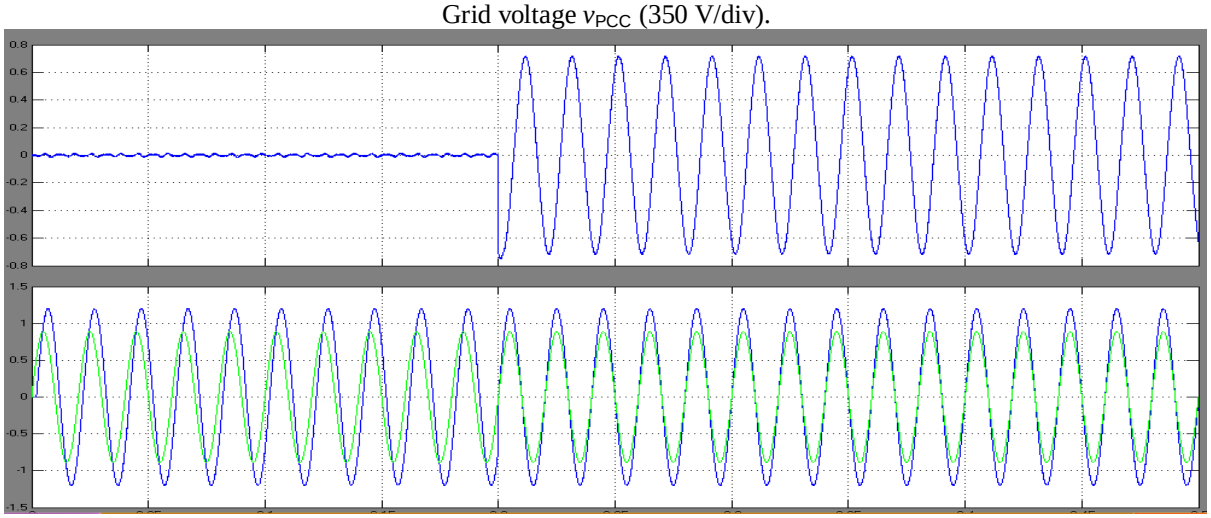

Fig. 19 Inverter transient response when only the reactive power compensation is enabled and the load is resistive–inductive. (Trace 1) Inverter current *iF* (10 A/div). (Trace 2) Grid current *iS* (10 A/div). (Trace 3) Grid voltage *v*PCC (350 V/div).

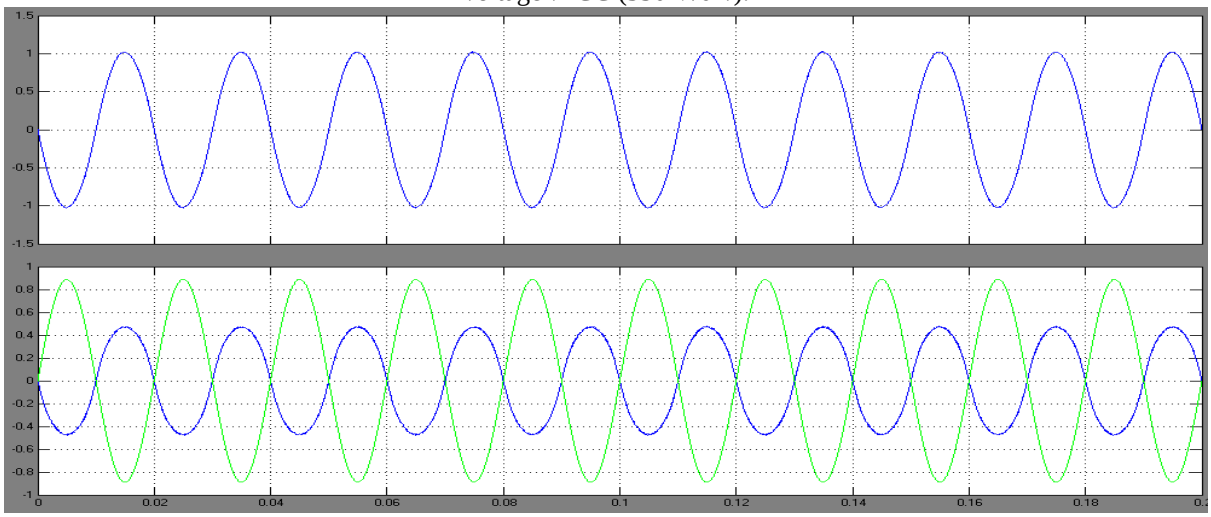

Fig. 20 Steady-state operation for 3 kWactive power generation with reactive power compensation. (Trace 1) Inverter current *iF* (20 A/div). (Trace 2) Grid current *iS* (10 A/div). (Trace 3) Grid voltage *v*PCC (350 V/div). (Trace A) Fourier analysis of the inverter current (0.5 A/div).

Finally, the transient response for step reactive power compensation when the generated active power was 3 kW is illustrated in Fig. 21, showing a time response of less than one grid period and no particular problems during the transient.

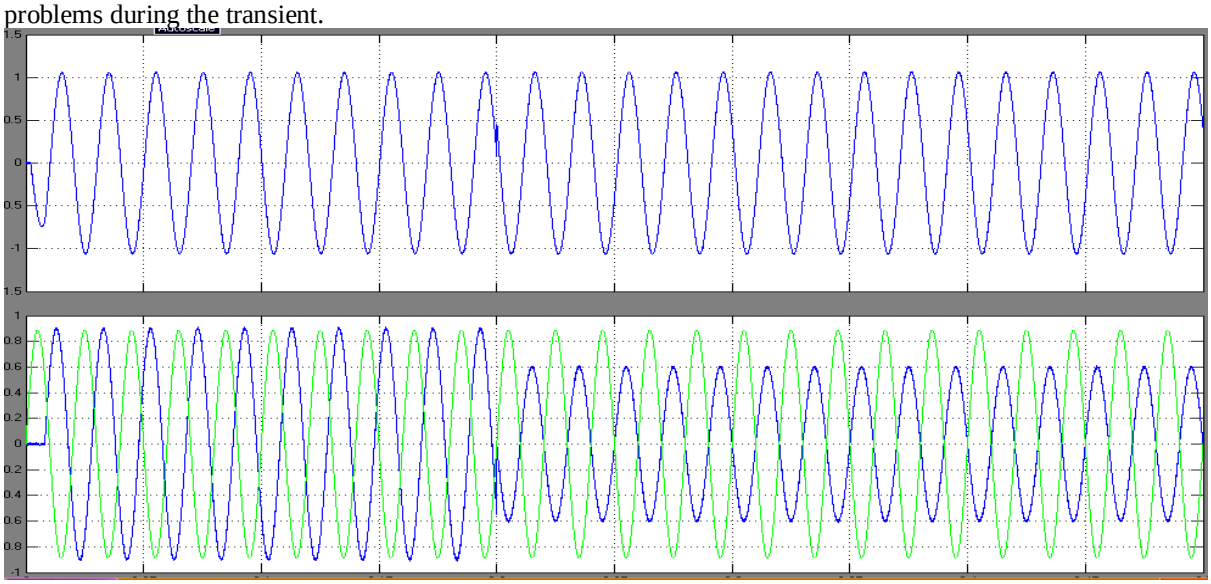

Fig. 21 Inverter transient response for step reactive power compensation when the injected active power is 3 kW. (Trace 1) Inverter current *iF* (20 A/div). (Trace 2) Grid current *iS* (10 V/div). (Trace 4) Grid voltage *v*PCC (350 V/div).

## IV. Conclusion

This paper deals with a single-phase H-bridge inverter for DG systems, requiring power quality features as harmonic and reactive power compensation for grid-connected operation. The proposed control scheme employs a current reference generator based on SSI and IRP theory, together with a dedicated repetitive current controller. The grid-connected single-phase H-bridge inverter injects active power into the grid and is able to compensate the local load reactive power and also the local load current harmonics. Simulation results have been obtained on a 4-kVA inverter prototype tested for different operating conditions, including active power generation, load reactive power compensation, and load current harmonic compensation. The experimental results have shown good transient and steady state performance in terms of grid current THD and transient response. The integration of power quality features has the drawback that the inverter will also deliver the harmonic compensation current with the direct consequence of increase the inverter overall current and cost. A current limitation strategy should be implemented and if the inverter output current exceeds the switch rating, then the supplied harmonic current must be reduced. In this way, the inverter available current is mainly used for active power injection and if there is some current margin, this can be used for the compensation of reactive power and nonlinear load current harmonics. An analysis of the inverter design that takes into account the current required for reactive power and current harmonics compensation is beyond the paper scope and it will be subject of future study.

## REFERENCES


[1] M. G. Villalva, J. R. Gazoli, and E. R. Filho, "Comprehensive approach to modeling and simulation of photovoltaic arrays," *IEEE Trans. Power Electron.*, vol. 24, no. 5, pp. 1198–1208, May 2009.

[2] B. Yang, W. Li, Y. Zhao, and X. He, "Design and analysis of a gridconnected photovoltaic power system," *IEEE Trans. Power Electron.*, vol. 25, no. 4, pp. 992–1000, Apr. 2010.

[3] Z. Chen, J. M. Guerrero, and F. Blaabjerg, "A review of the state of the art of power electronics for wind turbines," *IEEE Trans. Power Electron.*, vol. 24, no. 8, pp. 1859–1875, Aug. 2009.

[4] T. E. McDermott and R. C. Dugan, "Distributed generation impact on reliability and power quality indices," in *Proc. IEEE Rural Electr. Power Conf.*, 2002, pp. D3–D3_7.

[5] F. Blaabjerg, R. Teodorescu, M. Liserre, and A. V. Timbus, "Overview of control and grid synchronization for distributed power generation systems," *IEEE Trans. Ind. Electron.*, vol. 53, no. 5, pp. 1398–1409, Oct. 2006.

[6] F. Blaabjerg, Z. Chen, and S. B. Kjaer, "Power electronics as efficient interface in dispersed power generation systems," *IEEE Trans. Power Electron.*, vol. 19, no. 5, pp. 1184–1194, Sep. 2004.

[7] P. Rodriguez, A. V. Timbus, R. Teodorescu, M. Liserre, and F. Blaabjerg, "Flexible active power control of distributed power generation systems during grid faults," *IEEE Trans. Ind. Electron.*, vol. 54, no. 5, pp. 2583– 2592, Oct. 2007.

[8] L. P. Kunjumuhammed and M. K. Mishra, "Comparison of single phase shunt active power filter algorithms," in *Proc. IEEE Power India Conf.*, 2006, pp. 8–15.

[9] M. K. Ghartemani, H. Mokhtari, and M. R. Iravani, "A signal processing system for extraction of harmonics and reactive current of single phase systems," *IEEE Trans. Power Electron.*, vol. 19, no. 3, pp. 979–986, Jul. 2004.

[10] L. P. Kunjumuhammed and M. K. Mishra, "A control algorithm for singlephase active power filter under non-stiff voltage source," *IEEE Trans. Power Electron.*, vol. 21, no. 3, pp. 822–825, May 2006.
[11] M. T. Haque, "Single-phase pq theory for active filters," in *Proc. IEEE TENCON Conf. Rec.*, 2002, pp. 1941–1944.
[12] M. T. Haque, "Single-phase PQ theory," in *Proc. IEEE PESC Conf. Rec.*, 2002, pp. 1815–1820.
[13] M. T. Haque and T. Ise, "Implementation of single-phase pq Theory," in *Proc. IEEE PCC Conf. Rec.*, 2002, pp. 761–765.
[14] M. Saitou and T. Shimizu, "Generalized theory of instantaneous active and reactive powers in single-phase circuits based on Hilbert transform," in *Proc. IEEE PESC Conf. Rec.*, 2002, pp. 1419–1424.
[15] M. Saitou, N. Matsui, and T. Shimizu, "A control strategy of single-phase active filter using a novel d–q transformation," in *Proc. IEEE IAS Conf. Rec.*, 2003, pp. 1222–1227.
[16] J. Liu, J. Yang, and Z.Wang, "A new approach for single-phase harmonic current detecting and its application in a hybrid active power filter," *Proc. IEEE IECON Conf. Rec.*, pp. 849–854, 1999.
[17] Y. J. Kim, J. S. Kim, and Y. S. Kim, "Single-phase active power filter based on rotating reference frame method," in *Proc. IEEE ICEMS Conf. Rec.*, 2005, pp. 1428–1431.
[18] M. Gonzalez,V. Cardenas, and F. Pazos, "DQ transformation development for single-phase systems to compensate harmonic distortion and reactive power," in *Proc. IEEE CIEP Conf. Rec.*, 2004, pp. 177–182.
[19] S. M. Silva, B. M. Lopes, B. J. C. Filho, R. P. Campana, andW. C. Bosventura, "Performance evaluation of PLL algorithms for single-phase grid connected systems," in *Proc. IEEE IAS Conf. Rec.*, 2004, pp. 2259–2263.
[20] R. I. Bojoi, G. Griva, V. Bostan, M. Guerriero, F. Farina, and F. Profumo, "Current control strategy for power conditioners using sinusoidal signal integrators in synchronous reference frame," *IEEE Trans. Power Electron.*, vol. 20, no. 6, pp. 1402–1412, Nov. 2005.
[21] P. Rodriguez, R. Teodorescu, I. Candela, A. V. Timbus, M. Liserre, and F. Blaabjerg, "New positive-sequence voltage detector for grid synchronization of power converters under faulty grid conditions," in *Proc. IEEE PESC Conf. Rec.*, 2006, pp. 1–7.
[22] P. Mattavelli and F. P. Marafao, "Repetitive-based control for selective harmonic compensation in active power filters," *IEEE Trans. Ind. Electron.*, vol. 51, no. 5, pp. 1018–1011, Oct. 2004.
[23] L. R. Limongi, R. Bojoi, A. Tenconi, and L. Clotea, "Single-phase inverter with power quality features for distributed generation systems," in *Proc. IEEE OPTIM Conf. Rec.*, 2008, pp. 313–318.